Geophys. J. Int. (2007) **170,** 556–566 doi: 10.1111/j.1365-246X.2007.03432.x

Unmixing magnetic remanence curves without *a priori* knowledge

D. Heslop[1,2] and M. Dillon[1]

[1]*Department of Geosciences, University of Bremen,* P.O. Box 330 440*,* 28344 *Bremen, Germany*
[2]*Research Center Ocean Margins, University of Bremen,* 28334 *Bremen, Germany*

Accepted 2007 February 27. Received 2007 February 26; in original form 2006 October 6

SUMMARY

Many of the natural materials studied in rock and environmental magnetism contain a mixed assemblage of mineral grains with a variety of different origins. Mathematical decomposition of the bulk magnetic mineral assemblage into populations with different properties can therefore be a source of useful environmental information. Previous investigations have shown that such unmixing into component parts can provide insights concerning source materials, transport processes, diagenetic alteration, authigenic mineral growth and a number of other processes. A new approach will be presented that performs a linear unmixing of remanence data into coercivity based end-members using only a minimal number of assumptions. A non-negative matrix factorization (NMF) algorithm for unmixing remanence data into constituent end-members is described with case studies to demonstrate the utility of the approach. The shape of the end-members and their abundances obtained by NMF is based solely on the variation in the measured data set and there is no requirement for mathematical functions or type curves to represent individual components. Therefore, in contrast to previous approaches that aimed to unmix curves into components corresponding to individual minerals and domain states, NMF produces a genetically more meaningful decomposition showing how a data set can be represented as a linear sum of invariant parts. It has been found that the NMF algorithm performs well for both absolute and normalized remanence curves, with the capacity to process thousands of measured data points rapidly.

Key words: magnetic mixtures, non-negative matrix factorization, rock magnetism.

1 INTRODUCTION

The magnetic properties of any given mineral grain are controlled by a number of fundamental factors, such as composition, size, shape and stress (Dunlop & Özdemir 1997). The majority of environmental magnetic investigations are performed on bulk samples and therefore only measure a response integrated over the entire mineral assemblage. Given that many geological materials, for example marine sediments, contain a complex mixture of magnetic minerals with different environmental histories, the bulk response of a sample may provide ambiguous information. For a more complete enviromagnetic interpretation it is necessary to attempt to 'unmix' the behaviour of a given sample material in order to characterize the magnetic mineral assemblage. Such unmixing procedures attempt to decompose the magnetic signal into parts representing specific provenances that provide information on different environmental processes.

Coercivity spectra obtained by the stepwise acquisition or demagnetization of isothermal remanent magnetization (IRM) and anhysteretic remanent magnetization (ARM) curves often act as the basis for unmixing the magnetic mineral assemblages found in environmental materials. Based upon empirical evidence from well classified materials, Robertson & France (1994) hypothesized that bulk IRM acquisition curves could be modelled using a linear mixture of cumulative log-Gaussian (CLG) functions. The individual log-Gaussian elements contained in the model were assumed to represent independent coercivity components with different origins. A number of modelling procedures following this idea have been developed (Stockhausen 1998; Kruiver *et al.* 2001; Heslop *et al.* 2002) and the CLG approach has been applied in a wide variety of settings (Eyre 1996; Kruiver & Passier 2001; van Oorschot *et al.* 2002; Garming *et al.* 2005). Later experimental (Egli 2003) and theoretical (Egli 2004a; Heslop *et al.* 2004) work demonstrated that CLG functions were not sufficient to describe all remanence curves because shape properties, such as skewness and kurtosis were inherent to some coercivity distributions. The skewed generalized Gaussian (SGG) distribution introduced by Egli (2003) provided a more flexible function with which to model the demagnetization curves of ARMs. Both the skewness and the kurtosis of the SGG can be controlled, thus making it more suitable to the modelling of coercivity components that are not log-Gaussian. The applicability of the SGG function to modelling magnetic components has been demonstrated for magnetic populations with a number of provenances including aeolian dust (Spassov *et al.* 2003), urban pollution (Spassov *et al.* 2004), lake and marine sediments (Egli 2004b). Additional work performed by Egli (2004a) revealed a link between

the shape parameters of many coercivity distributions, indicating that kurtosis could be determined as an approximate function of skewness. Both the CLG and SGG approaches represent parametric techniques, which can be applied to single coercivity spectra and each defined component can be described using a relatively small number of parameters.

An alternative non-parametric approach to the unmixing problem is based on simultaneously decomposing a collection of remanence curves into components with constant properties, but varying abundances. Under these conditions such coercivity components can be thought of as end-members and a low-rank approximation of the data set is formed. A collection of methods proposed for such data modelling determine mixing abundances based upon *a priori* knowledge regarding the form of the individual end-members (Thompson 1986; Carter-Stiglitz *et al.* 2001). Therefore, before the unmixing can proceed, 'type curves' are required to represent the end-members. Given the large number of factors which can control the magnetic properties of an assemblage, it is unrealistic to assume that sufficient type curves could be collated to provide a representation of every possible end-member found in nature. An alternative approach is to consider each measured curve in the data set to be a potential end-member in order to find an optimal model (Shankar *et al.* 1994; Peters & Turner 1999). The applicability of such an approach is, however, limited to cases where the sample collection contains at least one pure example of each of the end-members in the mixing system.

The modelling procedure presented in this study uses linear combinations of end-members to represent coercivity spectra and thus does not rely on any specific distribution function. Unlike other end-member models, however, type curves are not required and there is no assumption that pure end-member curves must be contained in the measured data set. Instead, the method determines both the form of the end-members and their abundances using only the input remanence curves. The ideas behind this modelling procedure will be introduced, followed by two case studies that demonstrate the applicability of the method.

2 MAGNETIC ASSEMBLAGES AS LINEAR MIXTURES

The unmixing methods discussed in the previous section are all based on an assumption of linear additivity, however, the question as to whether such a property holds for magnetic mixtures remains open. Previous investigations have shown that magnetostatic interactions can produce non-linear effects in enviromagnetic procedures (Muxworthy *et al.* 2003, 2004; Carvallo *et al.* 2006; Muxworthy *et al.* 2006), but the extent of their influence in natural samples is still poorly understood. Magnetostatic interactions were detected by Heslop *et al.* (2006) in sediment suspensions with various compositions and concentrations, however, their effect was found to be minor. Experimental evidence from Lees (1997) demonstrated the possibility that modifying the magnitude of magnetostatic interactions in artificial mixtures would result in remanence curves that could only be explained with a non-linear mixing model. Using a preparation procedure to minimize grain clumping, Carter-Stiglitz *et al.* (2001) found linear additivity appeared to hold in artificial mixtures of variously sized magnetites.

For most mathematical unmixing procedures, it is assumed that whilst interactions between grains in the same magnetic component will not invalidate the linear model, the existence of magnetostatic interactions between the different components can produce non-linear behaviour. The success of previous unmixing studies based on a variety of different linear approaches provides at least some empirical evidence that the deviations from linear additivity due to magnetostatic interactions are minor in natural materials.

A number of previous studies have assumed that measured magnetization data resulted from a linear mixture of a number of invariant end-members (Shankar *et al.* 1994; Peters & Turner 1999; Carter-Stiglitz *et al.* 2001). A matrix $\mathbf{S}$ can be constructed to represent the form, that is, remanence curve, of each end-member. The matrix must therefore have one row for each of its m end-members and l columns spanning the applied field steps. A second matrix $\mathbf{A}$ represents abundances with n rows, one for the remanence curve of each measured sample and a column for each end-member. If $\mathbf{A}$ is interpreted in terms of abundances then it must be assumed that all of its values are non-negative, that is, $\mathbf{A} \geq 0$. Given an assumption of error-free perfect mixing, the data matrix $\mathbf{X}$ which is composed of n rows corresponding to the sample measurements, and l columns, corresponding to the measured field points, can be described by:

$$\mathbf{X} = \mathbf{AS}. \tag{1}$$

In practise, an observed matrix of remanence data will deviate from $\mathbf{X}$ due to measurement error and any non-linear effects, such as magnetostatic interactions between the components. Therefore, $\mathbf{X}$ will be composed of the remanence values explained by a linear model $\mathbf{AS}$ and an error kernel, $\boldsymbol{\epsilon}$:

$$\mathbf{X} = \mathbf{AS} + \boldsymbol{\epsilon}. \tag{2}$$

To form the data matrix $\mathbf{X}$, all the experimental remanence curves must be measured at the same field values, thus any column in $\mathbf{X}$ represents the remanences of the sample set at a single given field. For most real data sets this means it will be necessary to interpolate the measured curves onto a series of common field values. In addition $\mathbf{X}$ cannot be sparse, therefore it is necessary to have a remanence value for each curve at each field value.

In this study $\mathbf{A}$, $\mathbf{S}$ and $\boldsymbol{\epsilon}$ will be all considered as unknowns, and thus it is necessary to determine both the form of the magnetic coercivity components and their abundances using only the information contained in $\mathbf{X}$.

3 NUMERICAL UNMIXING PROCEDURE

To determine $\mathbf{A}$ and $\mathbf{S}$ numerically requires the definition of a cost function to provide a measure of the difference between the data $\mathbf{X}$ and the model matrix $\hat{\mathbf{X}}$ resulting from $\mathbf{AS}$. The squared Euclidean distance is adopted as a simple cost function which is optimal for systems that contain Gaussian distributed errors (Lee & Seung 2001):

$$\|\mathbf{X} - \hat{\mathbf{X}}\|^2 = \sum_{ij} (\mathbf{X}_{ij} - \hat{\mathbf{X}}_{ij})^2. \tag{3}$$

The key to solving the unmixing problem is the factorization of the matrix $\mathbf{X}$ in eq. (2), in such a manner that $\mathbf{A}$ and $\mathbf{S}$ can be determined simultaneously for a given number of end-members, that is, a specific value of m. To be appropriate to the unmixing problem, the factorization must be constrained in a variety of ways. First, the abundance values in $\mathbf{A}$ must be non-negative, thus $\mathbf{A} \geq 0$. Second, remanence acquisition is expected to proceed monotonically until saturation is achieved. A simple solution to this requirement is to process only remanence gradient data, as used in the gradient of acquisition plots (GAP) of by Kruiver *et al.* (2001). Using the GAP representation, the form of the end-members is expressed as the

derivative of the acquisition and can be constrained by $\mathbf{S} \geq 0$ to ensure monotonicity. To unmix linear or standardized acquisition data (LAP and SAP, respectively) would require more complex constraints to enforce monotonicity that will not be considered here. Finally the end-members in **S** should be linearly independent, in other words, it should not be possible to write any of the end-members as a linear combination of the other end-members.

Lee & Seung (2001) developed an iterative method of non-negative matrix factorization (NMF), to minimize $\|\mathbf{X} - \hat{\mathbf{X}}\|^2$ with respect to **A** and **S**, subject to the constraint $\mathbf{A}, \mathbf{S} \geq 0$, based on the multiplicative update rules:

$$S_{a\mu} \leftarrow S_{a\mu} \frac{(\mathbf{A}^{\mathrm{T}}\mathbf{X})_{a\mu}}{(\mathbf{A}^{\mathrm{T}}\mathbf{A}\mathbf{S})_{a\mu}}$$

$$A_{ia} \leftarrow A_{ia} \frac{(\mathbf{X}\mathbf{S}^{\mathrm{T}})_{ia}}{(\mathbf{A}\mathbf{S}\mathbf{S}^{\mathrm{T}})_{ia}}$$

where i, a, μ are the indices for the matrices, **A** and **S**, as $i = 1, \ldots, n, a = 1, \ldots, m$ and $\mu = 1, \ldots, l$. The multiplicative update rules will also fulfil the linear independence requirement of **S**. NMF can be applied to both absolute and normalized remanence curves, producing values of **A** that will be expressed in terms of absolute remanences and fractional abundances, respectively.

Lee & Seung (2001) provided a proof to show that under such a multiplicative update approach to NMF, the value of $\|\mathbf{X} - \hat{\mathbf{X}}\|^2$ would descend continually to at least a local minimum. The proof was later shown to be in error and it is possible for the NMF algorithm to descend to a saddle point (Berry *et al.* 2007). It is important to note therefore, that the NMF solution obtained by the presented multiplicative updates is not unique. NMF is still a developing field and recently a number of algorithms have been proposed based on adaptations of the Lee & Seung (2001) method to improve convergence properties (Cichocki *et al.* 2006a; Zdunek & Cichocki 2006).

To initialize the NMF algorithm, the user must define the number of end-members (m) to be included in the model and provide initial estimates of **A** and **S**. The majority of studies employing NMF simply initialize **A** and **S** using random numbers distributed uniformly in the interval [0, 1]. It has been demonstrated however, that the speed and accuracy of the solutions of NMF algorithms can be improved by providing good initializations based on the input data set (Wild *et al.* 2003; Langville *et al.* 2006). One example is to perform cluster analysis on **X** and use the locations of the cluster centres as the initial **S**. Using such an approach, the investigator would still be required to define the number of end-members manually by choosing the number of clusters to be calculated during the initialization procedure. Where appropriate **S** could be populated with predefined type curves, under the multiplicative updates **S** would not remain fixed, but in certain cases such an approach could provide a robust initialization leading to a meaningful convergence. Initializations could also employ CLG or SGG model solutions. For example, the average acquisition curve over an entire data set could be calculated and modelled using either the CLG or SGG methods, with the fitted functions providing an initial estimate of **S**. Using such an approach would still require an estimate of **A** for each measured sample, which given the estimate of **S**, could be found by solving a simple least-squares problem.

The entire iterative NMF algorithm including initialization and multiplicative updates can be written in a compact form using MATLAB® notation:

```
S = rand (m, l);
A = rand (n, m);
for i = 1 : maxiter
S = S. * (A'X)./(A'AS + eps);
A = A. * (XS')./(ASS' + eps);
end
```

where *eps* represents some small number, typically of the order 10^{-9} to avoid division by zero (Berry *et al.* 2007).

Here, the NMF approach is presented in its simplest form to demonstrate the applicability of such an approach to the unmixing of remanence curves. A large body of additional work exists, extending the basic NMF algorithm to employ alternative distance measures, control the smoothness of **A** and/or **S**, account for data sparseness and force ϵ to conform to a pre-defined distribution (Hoyer 2004; Cichocki *et al.* 2006a,b; Pauca *et al.* 2006; Zdunek & Cichocki 2006).

As a final point, it is important to consider the minimum number of measured curves that are required to obtain a robust model of the data, that is, what is the practical lower limit of n. This question is difficult to answer because it depends on various factors, such as the number of end-members to be fitted, the intersample variability in end-member abundance, the number of data points in the data curves and noise levels. In general, the investigator should attempt to include as many data curves as possible and run the algorithm a number of times starting from different initializations. Solutions that are clearly meaningless in a rock magnetic context can be discarded and the quality of the remaining solutions can be assessed by the ability to interpret them within the constraints of the specific scenario being investigated. If each separate initialization yields a similar result then it would appear that the algorithm is converging to a consistent minimum each time and the size of the input data set can be deemed to be sufficient. A series of numerical experiments with artificial and real data performed during the present study suggested that for typical remanence curves approximately 50 samples should be considered as the minimum value to ensure a robust unmixing.

3.1 Selecting an appropriate number of end-members

A problem common to remanence unmixing techniques is the decision of how many components should be included in the modelling procedure. A vast body of work exists concerned with the general ideas of model selection criteria (Burnham & Anderson 2002) and the general rules follow the idea that models should employ the minimum number of components that will still provide a good fit to the measured data. A key idea in this approach is that all the resolved components must be interpretable within the natural context of the data, a model which contains inexplicable components is thus deemed to be overly complex.

A number of statistical methods have been applied in the parametric unmixing of remanence data in an attempt to provide an objective estimation of the number of components that should be included in a model. Kruiver *et al.* (2001) adopted an approach based on the statistical testing of the distributions of residuals obtained from fitting with different numbers of CLG functions. An F-test was employed to compare the variance of the residuals from two different models involving m and $m + 1$ components. The more complex $m + 1$ model would be rejected if variance of the residuals from the calculated fit was not significantly lower than the residual variance from the m component model.

Egli (2003) adopted a different approach, employing Pearson's χ^2 goodness of fit test to determine the statistical similarity between measured data and a fitted SGG model. In terms of complexity, Egli (2003) recommended that a model is not overly complex if fitting with less parameters would produce a very different model result.

In this study, we propose a method which is less rigorous statistically than the approaches of Kruiver *et al.* (2001) and Egli (2003), but provides a clear visualization of differences between the measured data and the fitted model, aiding the determination of a suitable number of end-members for NMF models. The basis of the selection criterion lies in fact the NMF is applied to a collection of remanence curves simultaneously. Measured data and a resulting NMF model can be compared by the calculation of the coefficient of determination (r^2) between **X** and **AS** at each measured field value. This approach will provide a measure of how well a given model explains the data variance across the applied field range of the measurements. For the case of a model with insufficient end-members, the variance of the input data cannot be reproduced by the model and the calculated r^2 values will be low at a number of fields. For the optimum model, the r^2 value will be high across all the applied fields and it will be found that the inclusion of additional end-members will have little effect in improving the correlation between the measured and modelled data. The applicability of this approach will be demonstrated in the following case studies.

4 CASE STUDY I: NIGER FAN SEDIMENTS

Gravity core GeoB 4901 was recovered from the southern flank of the Niger deep-sea fan at a water depth of 2184 m. The sediments consisted mainly of clay-bearing diatomaceous nannofossil oozes, without any indications of perturbations (Zabel *et al.* 2001). A stable oxygen isotope chronological framework constructed for the core produced a basal age for the sediments of ∼245 ka, coincident with the transition between marine oxygen isotope stages 8 and 7 (Adegbie 2001).

Terrigenous material dominated the sediment composition, with variations reflecting the climatic history of central Africa, whilst carbonate content was generally low reaching a maximum value of ∼36 wt per cent. Terrigenous input was found to vary rhythmically with orbital parameters, reaching maxima during cold periods when decreased vegetation cover resulted in more intense physical erosion (Zabel *et al.* 2001). Geochemical studies of modern-day conditions indicated that the terrigenous component currently reaching the sampling location contained a maximum of 15 per cent aeolian material and thus was dominated by river-suspended matter. The location of the sampling site close to the Niger river mouth would suggest that a similar situation persisted throughout the history of the core with only minor contributions from aeolian components (Zabel *et al.* 2001).

A geochemical investigation of the core revealed that only the uppermost 10 cm of the sediments were oxic, additionally, based upon the appearance of hydrogen sulphide in the pore water the location of the suboxic/sulphidic transition was set at ∼12.5 m (Heuer 2003). The iron content of the sediment (mean iron concentration of 40.8 g kg^{-1}) was controlled by the lithogenic fraction as evidenced by a strong correlation with the aluminium concentration.

A detailed rock magnetic study of the diagenetically altered sediments from GeoB 4901 was reported recently by Dillon & Bleil (2006). Hysteresis, IRM, ARM, low temperature and thermomagnetic data were combined to provide a comprehensive interpretation of the sedimentary magnetic assemblage and its modification by a variety of diagenetic processes. Dillon & Bleil (2006) suggested that the vast majority of the magnetic assemblage reaching the core location was composed of eroded volcanic material originating from Cameroon. The volcanic assemblage was considered to be of variable composition, containing both titanomagnetites and titanohematites transported via the Niger tributaries. The presence of large numbers of volcanic grains in the sediment has since been confirmed by scanning electron micrographs and energy dispersive X-ray spectroscopy of selected samples.

The modern iron redox boundary was identified at a depth of ∼2.5 m on the basis of a sharp decrease in magnetic mineral content, Fig. 1(a), a shift to coarser grain sizes and a slight softening of the bulk coercivity (Dillon & Bleil 2006). Above the modern iron redox boundary, the ratio of κ_{ARM}/IRM is $\sim 2.0 \times 10^{-3}\ m/A$, which is high enough to be indicative of authigenic minerals including biogenic magnetite (Egli 2004b). Other studies have however reported similar values of κ_{ARM}/IRM from sediments where terrigenous input has been dominated by fine-grained (titano-)magnetites (Frank *et al.* 2003; Frank 2007). As mentioned above, Dillon & Bleil (2006) favoured a terrigenous origin for the magnetic assemblage, supporting their argument with low-temperature remanence data that showed no indication of a Verwey transition when measured on bulk samples and only a weak expression in magnetic extracts. It is however possible for the Verwey transition of bacterial magnetites to be suppressed if they form maghemite rims due to low-temperature oxidation (Smirnov & Tarduno 2000). Subsequent examination of larger terrigenous grains in scanning electron micrographs showed a minimal number of the surface cracks that could be taken as evidence for maghematization (Dunlop & Özdemir 1997), suggesting that the weak Verwey transition observed in the magnetic extracts was due to an absence of bacterial magnetites rather than surface oxidation of magnetosomes. Below the modern iron redox boundary relatively large amplitude variations are still observed in the concentration dependent parameters, beyond the suboxic/sulphidic transition however, these variations disappear and the parameters reach a baseline level.

The rock magnetic investigation of Dillon & Bleil (2006) showed that diagenetic alteration of the detrital titanomagnetites appears to have been dependant on both particle size and titanium content, with the smallest particles dissolving first and the Ti-rich component being the most resistant to the reducing conditions. In an attempt to trace the diagenetic history of the detrital assemblage, NMF unmixing was applied to a collection of 177 backfield curves which were measured during the original study of Dillon & Bleil (2006).

In order that they resembled IRM acquisition curves, the mass normalized backfield data were rescaled (division by a factor of 2), reversed and inverted (Fig. 1b). This pre-processing is necessary because NMF requires **X** to be non-negative, therefore converting backfield curves into pseudo-acquisition curves provides positive remanence values and assuming that the curves are monotonic, positive gradient values. In some cases, the measured curves were treated using a cubic smoothing spline (de Boor 1994), in order to reduce the influence of a relatively high noise contribution. To assess the effect of the smoothing procedure, the percentage residuals between the measured data and the smoothed data were calculated, (Fig. 2). The median of the residual distribution is found at ∼1 per cent, which represents a 1 per cent difference between the measured and smoothed data value. Some much larger residuals exist, in excess of 100 per cent, however they correspond to the very weak remanences where a small absolute change to the measured value during smoothing will produce a large percentage residual. Finally, the GAP

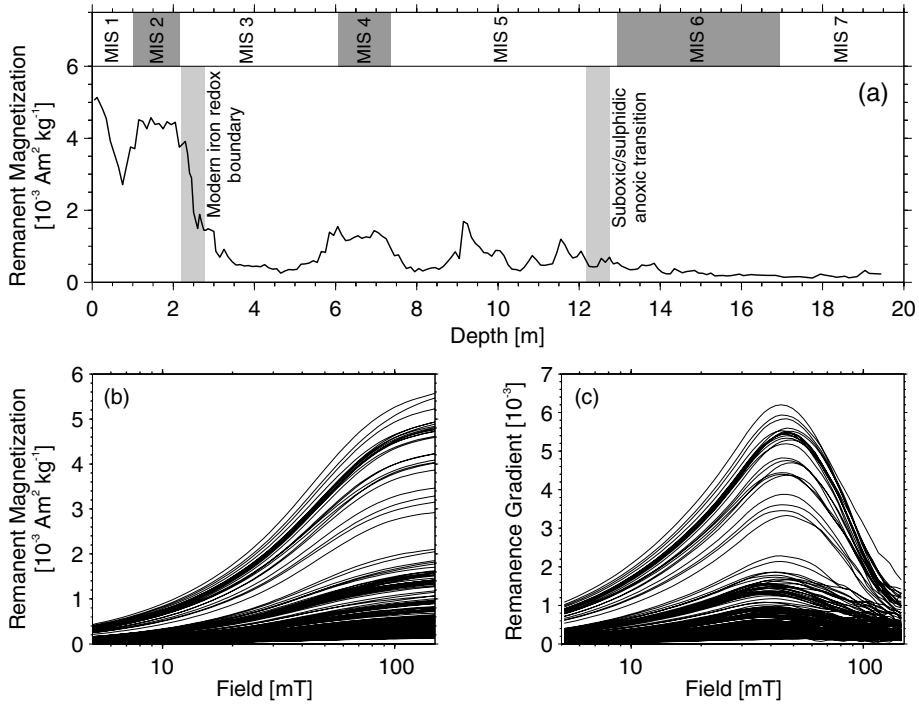

Figure 1. (a) Depth profile of the remanence acquired at 150 mT through the GeoB 4901 core with assigned Marine isotope stage (MIS) positions. (b) Smoothed remanence acquisition curves for all the samples in core GeoB 4901 based on the measured backfield data. (c) Remanence gradient data (GAP) calculated from the smoothed acquisition curves.

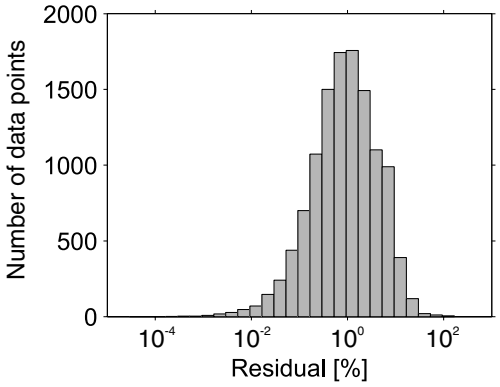

Figure 2. Percentage residuals of the smoothing procedure applied to the remanence curves of the Niger Fan sediments. The median residual is <1 per cent, however larger values are observed for the weak remanences.

data were calculated on a logarithmic field scale. It was found that a number of the GAP curves became noisy at higher fields, therefore the data matrix **X** was truncated at a maximum field of 150 mT (Fig. 1c). Saturated samples are not a requirement of the unmixing procedure, however, truncating the data at low fields will only allow the magnetically soft components of the mineral assemblage to be studied.

The number of end-members to be included in the model was based on the selection process described above. It is important to stress that, although the detrital flux reaching the core location is thought to have had a constant composition through time, the diagenetic processes did not act uniformly across the detrital magnetic mineral assemblage. Thus, a single end-member cannot be used to model the detrital magnetic mineral assemblage, but instead it is necessary to have multiple end-members in order to represent the relative abundance of different parts of the detrital assemblage as the diagenetic processes preferentially remove certain types of grains. It can be seen that a two component fit is not sufficient to model the measured data at a number of fields through the measured spectrum (Fig. 3a). A three component fit provides a great improvement at low fields, however some of the higher field data remains poorly modelled. The addition of an extra component in the 4 end-member model provides only a slight improvement at high fields, thus for the final unmixing, a 3 end-member model was selected. To initialize the NMF algorithm, a GAP model was calculated for a curve formed from the mean acquisition of all the samples, Fig. 3(b), given this estimate of **S**, a first estimate of **A** was made using constrained least squares.

The NMF model produces three negatively skewed distributions with similar forms to the SGG function proposed by Egli (2003). In the upper core, where the detrital assemblage is expected to be pristine, Fig. 4(a), end-member 2 (EM2) makes the greatest contribution to the remanence, followed by end-member 1 (EM1) and finally end-member 3 (EM3). The form of the end-members suggests that the magnetic assemblage is terrigenous in origin and not authigenic/bacterial. The softest two end-members have broad distributions and when modelled individually with SGG functions yield dispersion parameters >0.55, this property points towards a terrigenous origin and is incompatible with the small dispersion expected for bacterial magnetites because of their narrow grain size distributions (Kruiver *et al.* 2001; Egli 2004b). An extra analysis step which could provide additional insights into the data set would be to also perform unmixing of ARM data. In this way κ_{ARM}/IRM could be calculated for each end-member, providing clues to its origin. This idea was first demonstrated by Egli (2004b), who formed SGG models for both IRM and ARM curves and such an approach could be incorporated easily into the NMF procedure. Unfortunately, the ARM data measured for GeoB 4901 was not of sufficient resolution

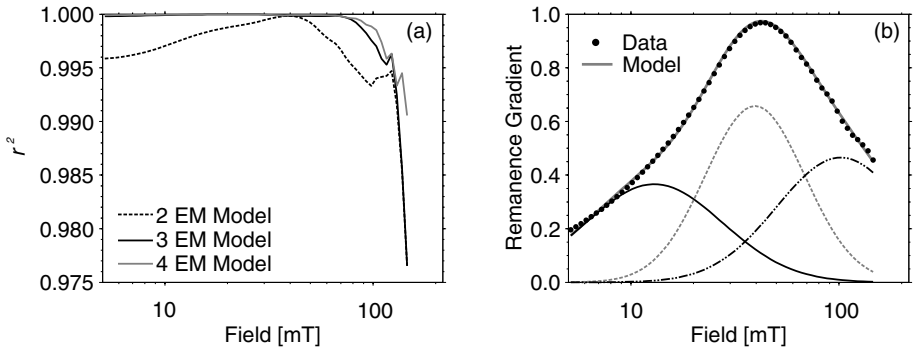

Figure 3. (a) Based on the correlation of the model and measured data as a function of applied field, a three end-member solution was selected as a balance between model quality and complexity. (b) A three component CLG model was formed for the mean acquisition curve to provide an initial **S**, the estimate of **A** for each sample was then obtained by constrained least squares. The CLG model (thick grey line) represents the linear addition of the individual log-Gaussian components and the mean GAP data is shown with closed symbols.

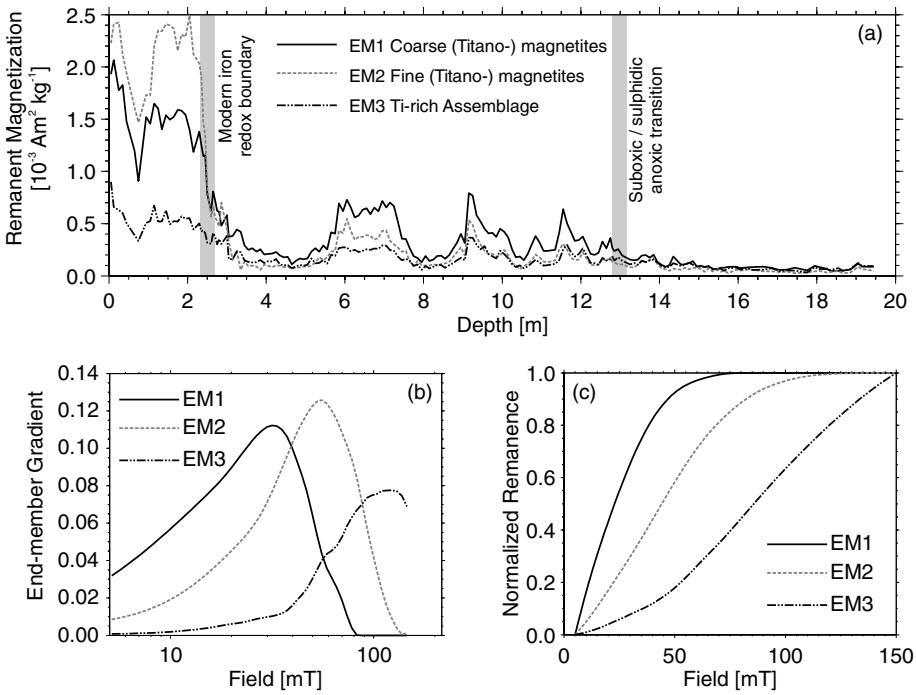

Figure 4. (a) Remanence contributions of the three individual end-members, note that both the absolute and relative proportions of the different end-members vary across the different diagenetic zones of the core. (b) Gradient curves produced as the NMF algorithm output **S**. (c) Remanence acquisition curves for the three end-members calculated from the output of the NMF algorithm. The end-members in **S** have been divided by factors to normalize each acquisition curve to a maximum value of one, absolute remanence values can be calculated for each end-member in each core position by multiplying **A** by the same factors. Because acquisition is non-linear it is not possible to extrapolate the normalized remanence of each end-member back to zero applied field.

to yield robust unmixing results, so interpretation had to be based solely on the backfield data.

At the modern iron redox boundary, a drop in the abundance of all three end-members is observed as dissolution occurs, however the rate at which the individual components decrease differs. A very gradual decrease in EM3 is observed across the modern iron redox boundary, in contrast EM1 is quicker, losing ∼93 per cent of its signal over ∼2.7 m. The greatest and most rapid decrease is seen in EM2, ∼98 per cent of its signal over ∼1.3 m, suggesting it is the end-member most susceptible to dissolution. Below the modern iron redox boundary, the largest contribution to the remanence is made by EM1.

Examination of the end-member coercivity distributions, Fig. 4(b), provides a explanation for the abundance behaviour which is consistent with the interpretation of Dillon & Bleil (2006). EM1 has a lower coercivity than EM2 and appears to have been more resistant to dissolution, this is thought to be a grain size effect, with EM1 composed of large (titano-)magnetite grains and EM2 composed of fine (titano-)magnetite grains which where more readily dissolved by the reducing conditions. It is apparent that EM3 had the greatest resistance to dissolution suggesting a Ti-rich titanomagnetite or titanohematite, this interpretation is supported by the slightly harder nature of this end-member (Day *et al.* 1977).

Below the suboxic/sulphidic transition, further changes are observed in the contributions of the end-members. Diagenetic processes act more slowly in anoxic conditions and all three end-members decrease gradually with depth reaching baseline values. Under certain redox conditions it is possible for new remanence

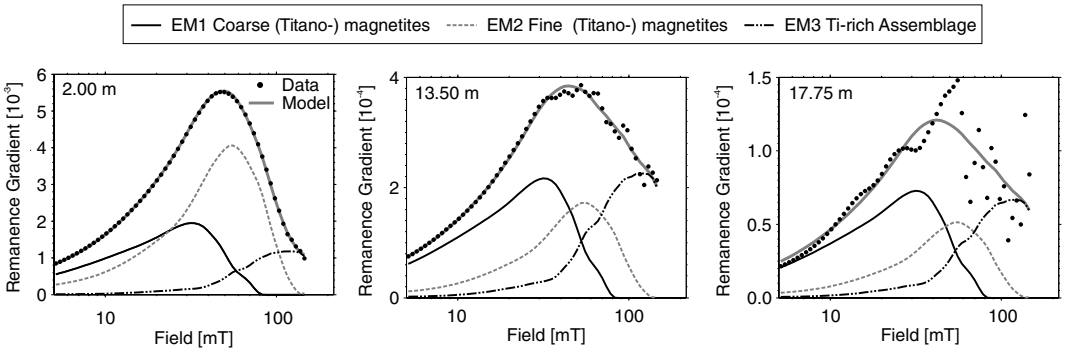

Figure 5. Individual sample fits for three locations through core GeoB 4901 that demonstrate the effect of diagenesis on the detrital input assemblage. In each case, the model (thick grey line) represents the linear addition of the individual end-members and the measured data is shown with closed symbols. The depth of the individual samples is shown in the top left corner of each panel.

bearing phases, such as greigite to be formed (Roberts & Turner 1993; Snowball & Torii 1999). Dillon & Bleil (2006) suggested that minor amounts of single-domain greigite may form in the anoxic zone of the sediments, if this is the case it is not detected in the unmixing, because even with the addition of an extra end-member, none of the resolved components could be interpreted as an authigenic iron sulphide phase.

Individual model fits for three sample horizons in the GeoB 4901 core are shown in Fig. 5. For the first sample (2.00 m), taken above the modern iron redox boundary, the detrital assemblage is dominated by contributions from the coarse and fine components (EM1 and EM2) and a good fit is observed between the data and the model. A sample taken from the lower part of the core (13.50 m), below the suboxic/sulphidic anoxic transition, shows dominant contributions from EM1 and EM3. A good model fit is still achieved when the absolute magnetizations are low, but the data degrades when moving towards high fields because of noise in the measured backfield curve. It is clear, however, that the model follows the general trend of the data and for such noisy curves it is not expected that each point can be fitted exactly. The final example comes from the sample with the worst fit (17.75 m), where there is little correspondence between the data and the model. It can be seen, however, that the data is very noisy, especially at higher fields, and it is not surprising that the model does not fit the data.

The Niger fan sediments can be used to demonstrate an additional point concerning end-member analysis. Because this form of unmixing focuses on forming a low-rank representation of the overall behaviour of a data set, it is possible that samples which deviate from the general pattern cannot be modelled properly. An example of this effect is observed below the modern iron redox boundary. A peak in the median destructive field of ARM was reported by Dillon & Bleil (2006) and attributed to the localized precipitation of bacterial magnetite. Because this zone has unique properties within the sediment sequence, it cannot be accurately modelled using an end-member approach. Shown in Fig. 6 is the data and model for the sample at 2.90 m which is believed to contain bacterial magnetite. A higher coercivity feature is clearly present in the 2.90 m sample, it cannot, however, be modelled with the three calculated end-members. In contrast, neighbouring samples at 2.80 and 3.00 m which are thought to not contain significant amounts of bacterial magnetite and have properties that are more typical of the sediment sequence as a whole can be fitted closely using the end-member model.

5 CASE STUDY II: A YOUNG MID-OCEAN RIDGE BASALT

The cooling rate gradient that exists between the glassy rim of a mid-ocean ridge basalt (MORB) pillow and its interior produces a spatial trend in titanomagnetite size and composition, which can be tracked by a number of rock magnetic procedures (Kent & Gee 1994; Pick & Tauxe 1994; Gee & Kent 1995, 1999; Fabian 2003, 2006). Rapidly cooled MORB samples commonly yield magnetization ratios (M_{rs}/M_s) greater than the value of 0.5 expected for

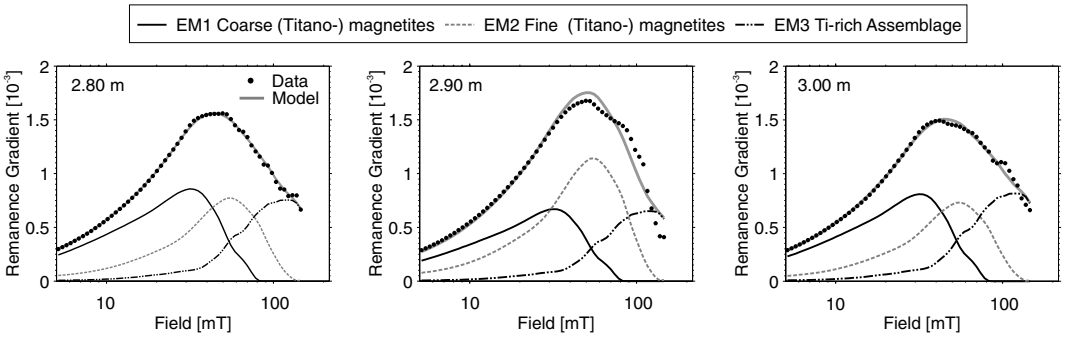

Figure 6. Sample fits spanning the sharp peak in median destructive field of ARM and attributed to bacterial magnetite. The samples above and below the peak, 2.80 and 3.00 m, respectively, can be fitted closely with the three end-member model. In contrast, the sample at the peak (2.90 m) has unique properties within the core and cannot be modelled properly using an end-member approach. In each case, the model (thick grey line) represents the linear addition of the individual end-members and the measured data is shown with closed symbols.

single domain grains dominated by uniaxial anisotropy (Stoner & Wohlfarth 1948). While some authors have suggested that such values are indicative of cubic anisotropy (Gee & Kent 1995, 1999), it has been demonstrated recently that values of $M_{rs}/M_s > 0.5$ were an experimental artifact and a uniaxial system will prevail for titanomagnetite in the presence of moderate internal stress (Fabian 2006).

A densely sampled zero age MORB from the Juan de Fuca Ridge forms the basis of this case study. Pillow specimen T787-R1 (provided by D. Kent) is ∼12 cm long and was cut perpendicular to the glassy margin, producing a transect to the pillow interior. The properties of this MORB have been measured in a number of previous studies and it is thought that the magnetic granulometric trend of the titanomagnetite assemblage is well understood (Zhou *et al.* 1997; Gee & Kent 1999; Zhou *et al.* 2000; Fabian 2003, 2006). Hysteresis loops measured by Fabian (2003) demonstrate the rapid cooling rate of the MORB at the chilled margin resulted in the formation of superparamagnetic (SP) and single-domain (SD) particles. The presence of SP grains is demonstrated by the reduced M_{rs}/M_s values at the rim of the MORB with values subsequently increasing as the SD grains begin to dominate the hysteresis behaviour (Fig. 8a). The slower cooling rate towards the interior of the pillow favoured the production of larger pseudo-single-domain (PSD) and multidomain (MD) particles. As in the previous case study, measured backfield curves (data provided by K. Fabian) were used in the unmixing procedure, therefore no information can be obtained concerning the contribution of SP particles. A total of 68 curves were prepared (rescaled, reversed, inverted and smoothed), however, no mass data were available, therefore the MORB data had to be normalized according to their maximum remanence. Sample locations are only available as positions, which vary only approximately linearly as a function of distance from the chilled margin of the specimen (Fabian 2003).

The composition of titanomagnetites ($Fe_{3-x}\ Ti_xO_4$; $0 \leq x \leq 1.0$) within an individual pillow can vary strongly depending on a number of factors controlled by the cooling rate. Combined magnetic and microscopy investigations (Zhou *et al.* 1997, 2000) identified a subset of titanomagnetite grains that grew up to 40 μm and increased in Ti content from $x \approx 0.3$ at the rim to $x \approx 0.6$ towards the interior of a pillow. A second subset of finer (SD to SP) particles revealed only a slight coarsening towards the interior and a highly variable Ti content ($0 \leq x \leq 0.8$) throughout the pillow.

The evolution of a titanomagnetite assemblage through a MORB pillow must be considered as dynamic and the first step is to determine how many end-members are required to provide a quantification of this behaviour through the T787-R1 specimen. All of the NMF models applied to the MORB data were initialized using only random numbers. We choose this form of initialization to demonstrate that in some cases a robust model can be obtained without a structured input for the NMF algorithm. Dunlop (2002) proposed that the PSD hysteresis properties of titanomagnetites could be modelled using a mixture of SD and MD behaviour. Given this proposition and the fact that SP material will play no role in remanence data, it is possible to imagine that the spatial variation of the magnetic properties within T787-R1 could be explained by a two end-member (SD and MD) model. The two-component model produced by the NMF algorithm yielded a poor fit to the data, this however is not surprising because the spatial evolution of the magnetic assemblage through a MORB pillow is complex. A comparison of 4, 5 and 6 end-member models reveals that sufficient complexity is achieved with a 5 end-member unmixing, Fig. 7, but little improvement is observed with six end-members.

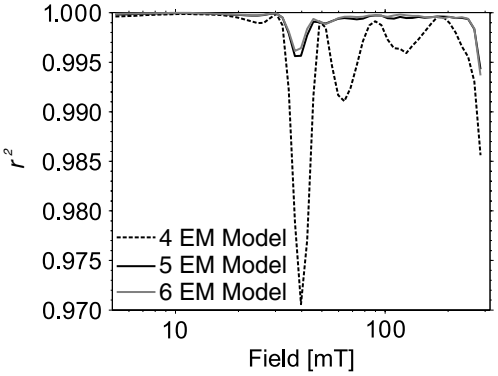

Figure 7. (a) Based on the correlation of the model and measured data as a function of applied field, a five end-member solution was selected as a balance between model quality and complexity. It can be seen that the five end-member solution provides a large improvement over the four end-member model, but the addition of extra components does little to further improve the model quality.

At the pillow interior, EM1 dominates the relative remanence contribution with values >75 per cent (Fig. 8b). Examination of the coercivity distribution, Figs 8(c) and 8(d), shows it is the softest component and reaches saturation just above 50 mT with a maximum in the coercivity spectrum at ∼30 mT. Such characteristics indicate that EM1 is composed of the large (MD) titanomagnetites, which were able to form in the more slowly cooled pillow interior. Based solely upon the coercivity spectrum, it is difficult to estimate the composition of the particles because there is no clear relationship between coercivity of remanence and the level of Ti substitution for coarse grained titanomagnetites (Day *et al.* 1977).

EM5 appears to be composed of particles with a broad distribution of coercivities, it is the hardest of the five components and does not saturate in a field of 300 mT. Because the NMF unmixing procedure is non-parametric, the derived coercivity distributions do not conform to a given mathematical function, therefore it is not possible to predict when a unsaturated component will reach saturation. Day *et al.* (1977) showed that the coercivity of remanence for fine wet-ground titanomagnetites was a function of composition, increasing by a factor of ∼4 from pure magnetite to $x = 0.6$. Such evidence suggests that EM5 represents a fine grained (SD) titanomagnetite assemblage with highly variable composition, possibly as high as $x = 0.8$, formed in the rapidly cooled outer part of the rim. Such a hypothesis is supported by the relative remanence contribution of EM5, which is highest (∼60 per cent) at the rim of the specimen and decreases to <10 per cent within ∼1.5 cm (assuming a linear relationship between position and distance).

EM2, EM3 and EM4 represent transitional assemblages that are required to explain the trends in grain size and composition which follow the cooling gradient of the pillow. It is important to note that because of the linear independence enforced by the NMF algorithm, the transitional end-members cannot be formed by simply mixing together EM1 and EM5. Instead, the transitional end-members allow for the non-linear behaviour of magnetic particle properties as a function of grain size and composition, and it is apparent that the PSD grains cannot be modelled simply as a linear combination of SD and MD behaviour. EM2 is more MD-like with a peak in its coercivity spectrum at ∼40 mT compared to the value of ∼100 mT for the more SD-like EM4. EM3 appears to be a true transitional assemblage with a coercivity peak at ∼55 mT and a shape which contains features similar to both the SD and MD components. Past

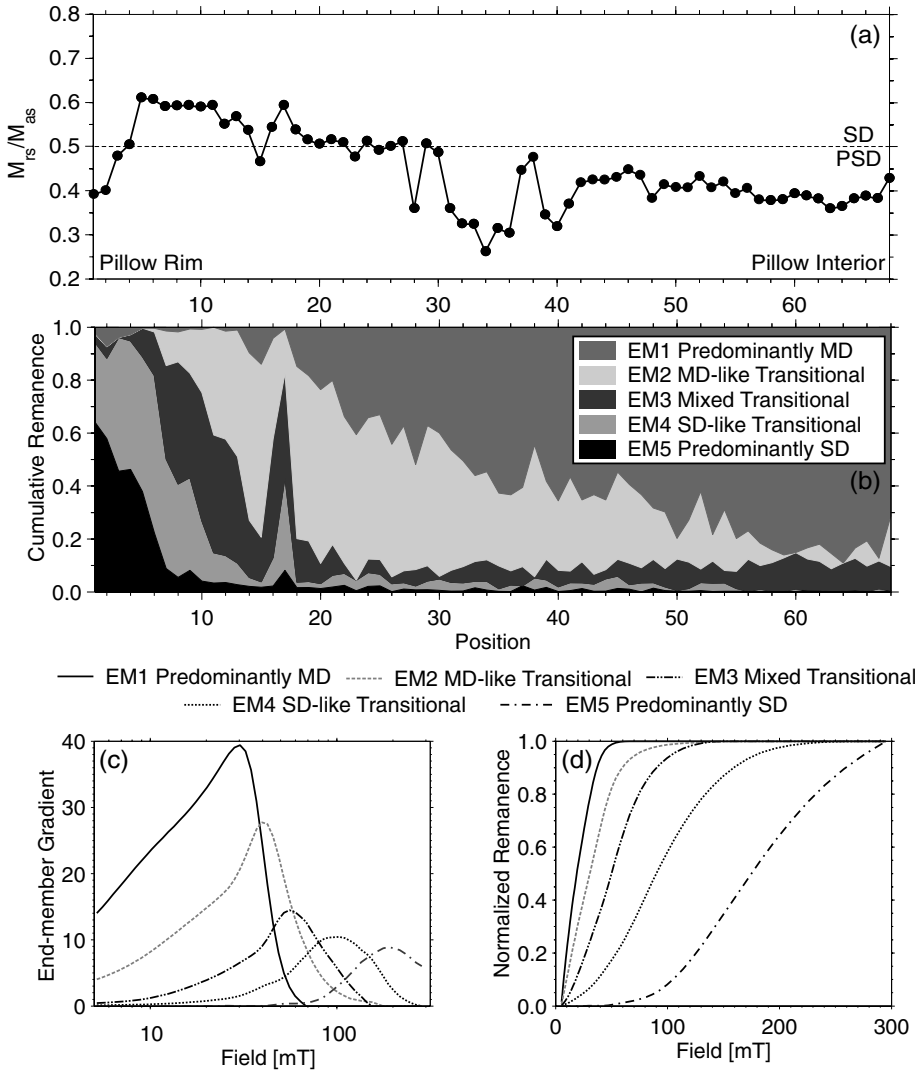

Figure 8. (a) Magnetization ratio measured across the zero age T787-R1 MORB specimen (data provided by K. Fabian). M_{as} corresponds to the 'apparent' saturation which does not take the high field (>1 T) behaviour of the samples into consideration. Sample positions along the ∼12 cm long specimen vary approximately linearly with distance from the chilled margin. (b) End-member abundances shown in a stacked area plot. The data set from T787-R1 was normalized, thus the end-member remanences can only be quoted in relative terms, with the contributions to each sample totalling one. (c) Gradient curves produced as the NMF algorithm output **S**. (d) Remanence acquisition curves for the four end-members calculated from the output of the NMF algorithm, the end-members in **S** have been divided by factors to normalize each curve to a maximum value of one.

a distance of ∼3 cm from the rim (corresponding to position 15 and assuming a linear relationship between position and distance), the SD dominated end-members have almost disappeared from the magnetic assemblage, making a <10 per cent combined contribution to the total remanence. At this position the MD-like components make a significant contribution to the remanence and gradually the full MD component (EM1) becomes dominant towards the interior of the pillow. The model fits for two samples are shown in Fig. 9 to demonstrate the shift from SD-type end-members at the pillow rim to MD-type end-members in the interior.

The presented case study demonstrates the ability of the NMF approach to unmix the variations in the magnetic assemblage of the T787-R1 MORB specimen. The description of the spatial variation of the magnetic properties provided by the end-member model corresponds clearly to the intrapillow processes described by previous authors. In cases, such as T787-R1 where the magnetic mineral inventory is seen to evolve gradually, it is necessary to derive a relatively large number of end-members in order that sufficient transitional assemblages can be defined to produce a good description of the measured data.

6 DISCUSSION AND CONCLUSIONS

The aim of this study was to demonstrate the potential of simple NMF algorithms to unmix remanent magnetization curves. The two presented case studies demonstrate the ability of such an approach to derive both coercivity components and their abundances based solely upon the variability in the measured data set. In the case of sediments from the Niger fan, the effects of diagenetic alteration on the detrital mineral assemblage could be traced in terms of both major changes across geochemical fronts and more gradual modifications as a function of depth. It was also possible to successfully model the evolving titanomagnetite population of the Juan de Fuca Ridge MORB by employing a relatively large number of end-members to

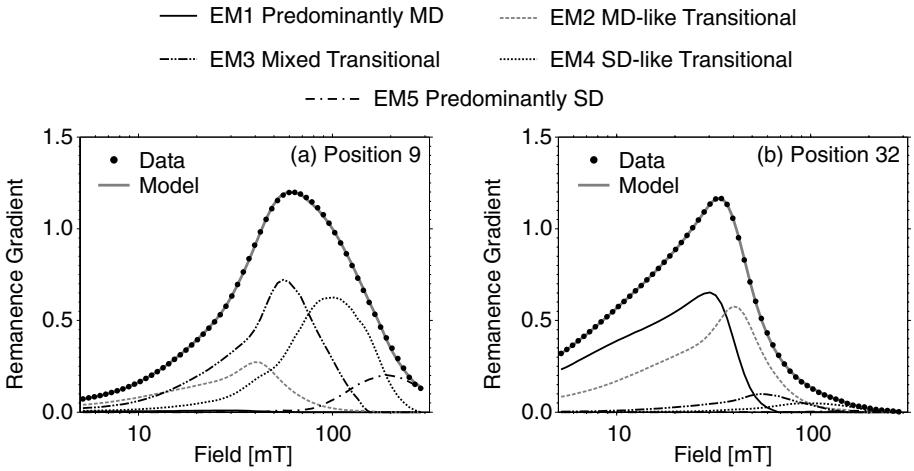

Figure 9. Data fits for two samples taken from the T787-R1 MORB specimen in positions 9 (pillow exterior) and 32 (pillow interior). (a) SD-type end-members are abundant towards the chilled margin of the MORB, whilst the MD end-member (EM1) makes only a very small contribution. (b) Towards the pillow interior, the lower coercivity MD-type end-members dominate whilst the SD end-members are almost entirely absent. In each case, the model (thick grey line) represents the linear addition of the individual end-members and the measured data is shown with closed symbols.

represent transitional assemblages. In both case studies, the number of end-members in each model was selected on the basis of the correlation between the measured and modelled data as a function of field. This approach does not involve statistical testing, but instead the selection criterion were only to keep the model simple, that is, adopting the minimum number of end-members that would provide a good fit to the data, and importantly the environmental origin and implications of each end-member had to be clear.

The potential of NMF based algorithms in the unmixing of rock and environmental magnetic data remains to be fully explored, in particular the question of initialization needs to be addressed in more detail. In principle, many types of magnetic data, both infield and remanence curves, could be analysed where a linear mixing model is thought to hold.

ACKNOWLEDGMENTS

The constructive reviews of M. J. Dekkers and R. Egli helped to improve the manuscript greatly. This work was funded by the DFG Research Centre "Ocean Margins" of the University of Bremen (contribution: 0487). The authors are grateful to K. Fabian who provided backfield data for the T787-R1 MORB specimen.

REFERENCES

Adegbie, A.T., 2001. Reconstruction of paleoenvironmental conditions in equatorial Atlantic and the Gulf of Guinea basins for the last 245 000 years, Tech. Rep. 178, Univ. Bremen, Bremen, Germany.

Berry, M., Browne, M., Langville, A., Pauca, P. & Plemmons, R., 2007. Algorithms and applications for approximate non-negative matrix factorization, *Comput. Stat. Data. Anal.,* in press, doi:10.1016/j.csda.2006.11.006.

Burnham, K.P. & Anderson, D.R., 2002. *Model Selection and Multimodel Inference: A practical Information-Theoretic Approach*, Springer-Verlag Inc, Berlin; New York.

Carter-Stiglitz, B., Moskowitz, B. & Jackson, M., 2001. Umixing magnetic assemblages and the magnetic behaviour of bimodel mixtures, *J. Geophys. Res.,* **106,** 26397–26411.

Carvallo, C., Muxworthy, A.R. & Dunlop, D.J., 2006. First-order reversal curve (FORC) diagrams of magnetic mixtures: Micromagnetic models and measurements, *Phys. Earth Planet. Inter.,* **154,** 308–322.

Cichocki, A., Amari, S., Zdunek, R., Kompass, R., Hori, G. & He, Z., 2006. Extended smart algorithms for non-negative matrix factorization, in *Artificial Intelligence and Soft Computing - ICAISC 2006*, Lecture Notes in Artificial Intelligence.

Cichocki, A., Zdunek, R. & Amari, S., 2006. Csiszar's divergences for non-negative matrix factorization: Family of new algorithms, *Independent component analysis and blind signal separation, Proceedings lecture notes in computer science,* **3889,** 32–39.

Day, R., Fuller, M. & Schmidt, V.A., 1977. Hysteresis properties of titanomagnetites: grain size and compositional dependence, *Phys. Earth Planet. Inter.,* **13,** 260–267.

de Boor, C., 1994. *A practical guide to splines*, Springer Verlag.

Dillon, M. & Bleil, U., 2006. Rock magnetic signatures in diagenetically altered sediments from the Niger deep-sea fan, *J. Geophys. Res.,* **111,** B03105.

Dunlop, D.J., 2002. Theory and application of the Day plot (Mrs/Ms versus Hcr/Hc) 1. Theoretical curves and tests using titanomagnetite data, *J. Geophys. Res.,* **107,** doi:10.1029/2001JB000486.

Dunlop, D.J. & Özdemir, Ö., 1997. *Rock magnetism: fundamentals and frontiers*, Cambridge University Press, Cambridge; UK.

Egli, R., 2003. Analysis of the field dependence of remanent magnetization curves, *J. Geophys. Res.,* **108**(B2), 2081.

Egli, R., 2004a. Characterization of individual rock magnetic components by analysis of remanence curves. 2. Fundamental properties of coercivity distributions, *Phys. Chem. Earth,* **29,** 851–867.

Egli, R., 2004b. Characterization of individual rock magnetic components by analysis of remanence curves, 1. Unmixing natural sediments, *Studia geoph. et geod.,* **48,** 391–446.

Eyre, J.K., 1996. The application of high resolution IRM acquisition to the discrimination of remenance carriers in Chinese loess, *Studia geoph. et geod.,* **40,** 234–242.

Fabian, K., 2003. Some additional parameters to estimate domain state from isothermal magnetization measurements, *Phys. Earth Planet. Inter.,* **213,** 337–345.

Fabian, K., 2006. Approach to saturation analysis of hysteresis measurements in rock magnetism and evidence for stress dominated magnetic anisotropy in yound mid-ocean ridge basalt, *Phys. Earth Planet. Inter.,* **154,** 299–307.

Frank, U., 2007. Rock magnetic studies on sediments from Erlongwan maar lake, Long Gang Volcanic Field, Jilin province, NE China, *Geophys. J. Int.,* **168,** 13–26.

Frank, U., Schwab, M.J. & Negendank, J.F.W., 2003. Results of rock magnetic investigations and relative paleointensity determinations on lacustrine sediments from Birkat Ram, Golan Heights (Israel), *J. Geophys. Res.,* **108**(B8), 2379.

Garming, J.F.L., Bleil, U. & Riedinger, N., 2005. Alteration of magnetic mineralogy at the sulphate–methane transition: Analysis of sediments

from the Argentine continental slope, *Phys. Earth Planet. Inter.,* **151,** 290–308.

Gee, J. & Kent, D.V., 1995. Magnetic hysteresis in Young midocean ridge basalts: dominant cubic anisotropy?, *Geophys. Res. Lett.,* **22,** 551–554.

Gee, J. & Kent, D.V., 1999. Calibration of magnetic granulometric trends in oceanic basalts, *Phys. Earth Planet. Inter.,* **170,** 377–390.

Heslop, D., Dekkers, M.J., Kruiver, P.P. & van Oorschot, I.H.M., 2002. Analysis of isothermal remanent magnetization acquisition curves using the expectation-maximization algorithm, *Geophys. J. Int.,* **148,** 58–64.

Heslop, D., McIntosh, G. & Dekkers, M.J., 2004. Using time and temperature dependant Preisach models to investigate the limitations of modelling isothermal remanent magnetisation curves with cumulative log Gaussian functions, *Geophys. J. Int.,* **157,** 55–63.

Heslop, D., Witt, A., Kleiner, T. & Fabian, K., 2006. The role of magnetostatic interactions in sediment suspensions, *Geophys. J. Int.,* **165,** 775–785.

Heuer, V., 2003. Spurenelemente in Sedimenten des Südatlantik: Primärer Eintrag und frühdiagenetische Überprägung, Tech. Rep. 209, Univ. Bremen, Bremen, Germany.

Hoyer, P.O., 2004. Non-negative matrix factorization with sparseness constraints, *J. Mach. Learn. Res.,* **1457,** 1457–1469.

Kent, D.V. & Gee, J., 1994. Grain size dependent alteration and the magnetization of oceanic basalts, *Science,* **265,** 1561–1563.

Kruiver, P.P. & Passier, H.F., 2001. Coercivity analysis of magnetic phases in sapropel S1 related to variations in redox conditions, including an investigation of the S-ratio., *Geophys. Geochem. Geosyst.,* **2,** doi:10.1029/2001GC000181.

Kruiver, P.P., Dekkers, M.J. & Heslop, D., 2001. Quantification of magnetic coercivity components by the analysis of acquisition curves of isothermal remanent magnetization, *Earth Planet. Sci. Lett.,* **189,** 269–276.

Langville, A.N., Meyer, C.D. & Albright, R., 2006. Initializations for the nonnegative matrix factorization, in *Proceedings of the Twelfth ACM SIGKDD International Conference on Knowledge Discovery and Data Mining*.

Lee, D.D. & Seung, H.S., 2001. Algorithms for non-negative matrix factorization, *Adv. Neural Inform. Process. Syst.,* **13,** 556–562.

Lees, J.A., 1997. Mineral magnetic properties of mixtures of environmental and synthetic materials: linear additivity and interaction effects, *Geophys. J. Int.,* **131,** 335–346.

Muxworthy, A.R., Williams, W. & Virdee, D., 2003. Effect of magnetostatic interactions on the hysteresis parameters of single-domain and pseudo-single-domain grains, *J. Geophys. Res.,* **108,** doi:10.1029/2003JB002588.

Muxworthy, A.R., Heslop, D. & Williams, W., 2004. Influence of magnetostatic interactions on first-order reversal curve (FORC) diagrams: a micromagnetic approach, *Geophys. J. Int.,* **158,** 888–897.

Muxworthy, A.R., King, J.G. & Odling, N., 2006. Magnetic hysteresis properties of interacting and non-interacting micron-sized magnetite produced by electron-beam lithography, *Geophys. Geochem. Geosyst.,* **7**.

Pauca, V.P., Piper, J. & Plemmons, R.J., 2006. Non-negative matrix factorization for spectral data analysis, *Lin. Algebra Appl.,* **416,** 29–47.

Peters, C. & Turner, G., 1999. Lake Paringa: a catchment study using magnetic techniques, *Phys. Chem. Earth,* **24,** 753–757.

Pick, T. & Tauxe, L., 1994. Characteristics of magnetite in submarine basaltic glass, *Geophys. J. Int.,* **119,** 116–128.

Roberts, A.P. & Turner, G.M., 1993. Diagenetic formation of ferrimagnetic iron sulphide minerals in rapidly deposited marine sediments, South Island, New Zealand, *Earth Planet. Sci. Lett.,* **115,** 257–273.

Robertson, D.J. & France, D.E., 1994. Discrimination of remanence carrying minerals in mixtures, using isothermal remanent magnetization aquisition curves, *Phys. Earth Planet. Inter.,* **82,** 223–234.

Shankar, R., Thompson, R. & Galloway, R.B., 1994. Sediment source modelling: Unmixing of artifical magnetization and natural radioactivity measurements, *Earth Planet. Sci. Lett.,* **126,** 411–420.

Smirnov, A.V. & Tarduno, J.A., 2000. Low-temperature magnetic properties of pelagic sediments (Ocean Drilling Program Site 805C): Tracers of maghemitization and magnetic mineral reduction, *J. Geophys. Res.,* **105,** 16457–16471.

Snowball, I.F. & Torii, M., 1999. *Quaternary Climates and Magnetism*, chap. Incidence and significance of ferrimagnetic iron sulphides in Quaternary studies, pp. 199–230, Cambridge University Press.

Spassov, S., Heller, F., Kretzschmar, R., Evans, M.E. & Nourgaliev, L.P.Y. D.K., 2003. Detrital and pedogenic magnetic mineral phases in the loess/palaeosol sequence at Lingtai (Central Chinese Loess Plateau), *Phys. Earth Planet. Inter.,* **140,** 255–275.

Spassov, S., Egli, R., Heller, F., Nourgaliev, D.K. & Hannam, J., 2004. Magnetic quantification of urban pollution sources in atmospheric particulate matter, *Geophys. J. Int.,* **159,** 555–564.

Stockhausen, H., 1998. Some new aspects for the modelling of isothermal remanent magnetization acquisition curves by cumulative log Gaussian functions, *Geophys. Res. Lett.,* **25,** 2217–2220.

Stoner, E.C. & Wohlfarth, E.P., 1948. A mechanism of magnetic hysteresis in heterogeneous alloys, *Phil. Trans. Roy. Soc.,* **240,** 599–642.

Thompson, R., 1986. Modelling magnetization data using SIMPLEX, *Phys. Earth Planet. Inter.,* **42,** 113–127.

van Oorschot, I.H.M., Dekkers, M.J. & Havlicek, P., 2002. Selective dissolution of magnetic iron oxides with the acid-ammonium-oxalate/ferrous-iron extraction technique - II. Natural loess and palaeosol samples, *Geophys. J. Int.,* **149,** 106–117.

Wild, S., Curry, J. & Dougherty, A., 2003. Motivating non-negative matrix factorizations, in *Proceedings of the eighth SIAM conference on applied linear algebra*.

Zabel, M., Schneider, R.R., Wagner, T., Adegbie, A.T., de Vries, U. & Kolonic, S., 2001. Late Quaternary climate changes in central Africa as inferred from terrigenous input to the Niger Fan, *Quat. Res.,* **56,** 207–217.

Zdunek, R. & Cichocki, A., 2006. Non-negative matrix factorization with quasi-Newton optimization, in *Artificial Intelligence and Soft Computing - ICAISC 2006*, Lecture Notes in Artificial Intelligence.

Zhou, W., van der Voo, R. & Peacor, D.R., 1997. Single-domain and superparamagnetic titanomagnetite with variable Ti content in young ocean-floor basalts: No evidence for rapid alteration, *Earth Planet. Sci. Lett.,* **150,** 353–362.

Zhou, W., van der Voo, R., Peacor, D.R. & Zhang, Y., 2000. Variable Ti-content and grain size of titanomagnetite as a function of cooling rate in very young MORB, *Earth Planet. Sci. Lett.,* **179,** 9–20.